# Physico-chemical Characterization of Different Preparation Routes of Binary and Ternary Metal Oxides on Titanium Substrates

*Michael J. Klink[1], Eno E. Ebenso[1,*], Andrew M. Crouch[2]*

[1] Department of Chemistry, School of Mathematical and Physical Sciences, North-West University (Mafikeng Campus), Private Bag X2046, Mmabatho 2735, South Africa
[2] Institute of Molecular Sciences, School of Chemistry, Faculty of Science, University of the Witwatersrand, Private Bag 3, Johannesburg, 2050, South Africa
[*]E-mail: Eno.Ebenso@nwu.ac.za

Different routes of preparation of metal oxide structures on titanium substrates are explored and characterized with Scanning Electron Microscopy (SEM), Energy Dispersive Elemental Analysis (EDAX), Atomic Force Microscopy (AFM) and X-ray Diffraction Spectroscopy (XRD). The aim was to look for alternative material breakthroughs and to promote the conductivity and the compatibility of the electrode by increasing the surface area of the electrode which will then increase the catalytic efficiency. The SEM and AFM micrographs showed different micro- and nano-structured morphologies for the electrodes. The XRD distinctively identified the presence of crystalline structures of $IrO_2$, $SnO_2$ and ZnO modified electrodes.

## 1. INTRODUCTION

The advances in microelectronics material technology have been driven by the need to fabricate increasingly smaller material devices to create integrated circuits with improved performance and architecture. However, while continuously miniaturizing devices dimension, the existing materials are approaching their physical limits and inevitably looking for alternative material breakthroughs. These materials must be nano-scale, physically and chemically stable materials, thus offering new opportunities to complement the electronic material technology. The down scaling of the material dimension not only implies a shrinkage of the active device which leads to higher packing density and

lower power consumption, but also can significantly improve the device performance [1-3]. Metal oxides constitute the most common, most diverse and fascinating class of materials in terms of electronic structure and physical, chemical and structural properties. Their properties range from insulating to semi-conductors, conductors or magnetic behaviors with transitions among those states. As a group of functional materials, metal oxides have a wide range of applications, including transparent electronics, (chemical-, gas-, bio) sensors, piezoelectric transducers, light-emitting devices, fuel cells, solar cells, support for catalysts etc. The diversity of such applications originates from the more complex crystal and electronic structures compared to other class structures. The main reasons are related to their variety of oxidation states, coordination number, symmetry, ligand-field stabilization, density, stoichiometry and acid-base properties [5-6].   As research progressed, it was found that mixtures of these metal oxides showed even more unique properties. The range of such compounds is quite large, but is extended even further by considering ternary and yet more complex compounds, where additional interesting properties are present [7-8]. The catalytic properties of existing known metal oxide catalysts can be enhanced by tailoring their micro- and nanostructure. They may come in the form of either new oxides or new composite materials containing polymers and oxide blends or the new properties associated with nano-structured materials. Recent studies have shown that the electro-catalytic activity and chemical or mechanical stability of oxide electrodes are enhanced by incorporating/ doping other metal ions into the oxides [9]. In this study, we report the studies on metal oxide mixtures (binary, ternary, etc.) in the form of micro-, nano-materials and sol-gel films developed by different routes and characterized using scanning electron microscopy (SEM), energy dispersed analysis of x-rays (EDAX), atomic force microscopy (AFM) and x-ray diffractometry (XRD).

## 2. EXPERIMENTAL

### 2.1 Chemicals

$TaCl_5$, $RuCl_3$, $SnCl_2$, $RhCl_3$, $IrCl_3$, $Na_2HPO_4$, $NaNO_3$, $C_6H_{12}N_4$, $Zn(NO_3)_2 \cdot 6H_2O$ and Ti foil were obtained from Aldrich Chemicals (Germany).  Absolute ethanol, methanol, potassium chloride, potassium ferricyanide and hydrochloric acid obtained from Merck were used in the experiments. Phosphoric acid (85 % in water) from Sigma-Aldrich and sodium fluoride (99.5%) from Fisher were also used. All reagents were of analytical grade and were used without further purification.

### 2.2 Preparation of sol-gel mixed metal oxide structures on titanium substrates

The titanium substrates, for all the different routes, were cut to size (1 cm × 1 cm), sandblasted and etched in HCl (11.5 M) for 5 minutes, rinsed with copious amounts of ultrahigh quality water and finally rinsed with absolute ethanol and dried with air.

Route (i): An electrical connection was made through a Cu wire welded to the titanium substrate using silver epoxy. For the electrical anodization of the Ti metal substrate, a DC power

supply was used. Constant voltage anodization was carried out using a two electrode configuration with a working electrode made of Ti metal sheet and a counter electrode made of Pt wire. All experiments were conducted at room temperature and at an applied voltage of 20 V for 1 hr. The distance between the anode and cathode was kept at about 3 cm. A mixture of 0.5 M $H_3PO_4$ and 0.14 M NaF solution was used as electrolyte for the electrochemical anodic reaction and the pH was adjusted to between 1.5 and 5 by adding NaOH or KOH. The electrolyte was stirred continuously at ~ 150 rpm using a magnetic stirrer. The anodized samples were washed and sonicated in distilled water for 5 minutes to remove the remnants on the surface and then blown dry in an air stream. In order to improve the crystalline properties and remove remnants or barrier oxide layer after the anodic reaction, the as-anodized samples were annealed at 500 °C for 2 h under air ambient [10].

Route (ii): The metal oxide particles were synthesized based on procedures reported in literature [11-13]. An aqueous solution (milliQ, 18.2 MΩcm) of equimolar Zn $(NO_3)_2 \cdot 6H_2O$ and $C_6H_{12}N_4$, $NaNO_3$ and $C_6H_{12}N_4$ were put in a glass bottle with a screw cap. The titanium substrates were placed in the bottle with the aqueous precursors and heated at a constant temperature at 95 – 100 °C for 24 hrs in a regular laboratory oven. Subsequently, the substrates were thoroughly washed with milliQ water to eliminate residual salts and dried in air at a similar temperature.

Route (iii): A sol–gel synthesis for the metal oxides titanium materials based on procedures modified from literature was used in the experiments [14-15]. The starting materials were placed in a round bottomed flask fitted with a thermometer, and the solutions were well stirred and refluxed for 1 h, before being left to age at room temperature for at least 24 h to ensure ageing of the gel. For the purpose of producing the thin films, the gels were retained in the liquid form. Two to three drops of the respective gel material were put on the Ti substrate, fixed to a rotating disk surface and rotated at full speed (~ 1000 rpm) for 10 s to give reproducible thin films after which it were put in an oven at 70 – 80 °C for 20 minutes after each drop respectively. The thin films were then annealed in an oxygen-rich atmosphere in a quartz tube furnace at a slow heating rate (1 °C/min) up to 700 °C and then allowed to cool to room temperature, under ambient conditions after which oxidation was performed as in route (i).

Route (iv): This is a mixture of procedures of routes (iii) and (i).


## 2.3 Techniques

### 2.3.1. Scanning electron microscopy (SEM) and Energy dispersive analysis of x-rays (EDAX)

The surface morphologies of the electrodes were analyzed using SEM. An ABT60 Scanning Electron Microscope complimented by elemental X-ray analysis (EDAX) was used for the experiments.

The SEM pictures were taken at a working distance of 7 mm and an accelerating voltage of 7 kV. The samples were placed horizontally on the stubs and they were not coated for viewing. For the X-ray analysis, the working distance was 12 mm and the accelerating voltage was 25 kV. The samples were tilted at 30 degrees..

*2.3.2 Atomic Force Spectroscopy (AFM)*

Atomic force microscopy (AFM) micrographs were taken at two different positions on each thin film (solid state) that was prepared using a Nanoscope IIIa dimension 3000/100 Veeco Microscope. The samples were scanned in non-contact mode (i.e. the probe was oscillated in the attractive regime). A low resonance frequency cantilever was used and the force spring constant was 35–65 N/m.

*2.3.3 X-ray Diffraction (XRD)*

The electrode surface was characterized by XRD using a D8 Advance powder diffractometer with a theta-theta goniometer. The X-ray source was a copper tube and a NaI (Tl) scintillation detector that detected the diffracted beam. The film surface was oriented perpendicular to a plane defined by the X-ray tube, sample holder and detector.

## 3. RESULTS AND DISCUSSION

*3.1 SEM analyses of the different metal oxides on titanium substrates*

Figure 1 shows self-ordered nano-pores or holes with large surface area when Ti foil was anodized in strong acids (0.5 M $H_3PO_4$ + 0.14 M NaF) for 5 hrs at a constant potential of 20 V (Route (i)). The insert micrograph shows at a particular time when all the smooth Ti areas were not all oxidized. We therefore clearly see that the pitting of the Ti substrate was not finished. $TiO_2$ nano-pores with a broad range of scales between $20 - 120$ nm and an inner diameter wall of $5 - 15$ nm inner circle thickness were observed in the bigger micrograph. The mechanisms for the formation and growth of the $TiO_2$ nano-circle structure have been reported extensively and remain the subject of some debate. It is believed that the nano-pores formation is driven by the competition between two electric field assisted processes: (i) oxidation of Ti to form $TiO_2$ and (ii) chemical dissolution of $TiO_2$ at the $TiO_2$/electrolyte interface [16-17]:

$$Ti + 2H_2O \rightarrow TiO_2 + 4H^+ + 4e^- \qquad (1)$$

$$TiO_2 + 6HF \rightarrow [TiF_6]^{2-} + 2H_2O + 2H^- \qquad (2)$$
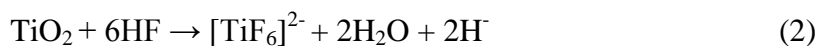
The oxide microstructure typically evolves through four stages: (i) formation of a dense barrier oxide layer (eq (1)) [17-19]; chemical dissolution of $TiO_2$ to form cylindrical nanopores (by Eq. (2)) [16-19]; (iii) development of a bilayered structure consisting of a nanotube layer covered by the nanoporous layer and (iv) dissolution of the nanoporous layer resulting in nanotube structure. The nanotubes are however not seen in the SEM micrographs since a cross dissection was not performed. Crawford and Chwala [20] reported that the rate of the nanotube formation is controlled by the

crystallographic orientation of the Ti surface. The authors conclude that the anodic oxidation is strongly affected by the orientation of the Ti substrate, that the growth is retarded when the close-packed plane is parallel to the Ti surface, which is related to the higher atomic density of the plane.
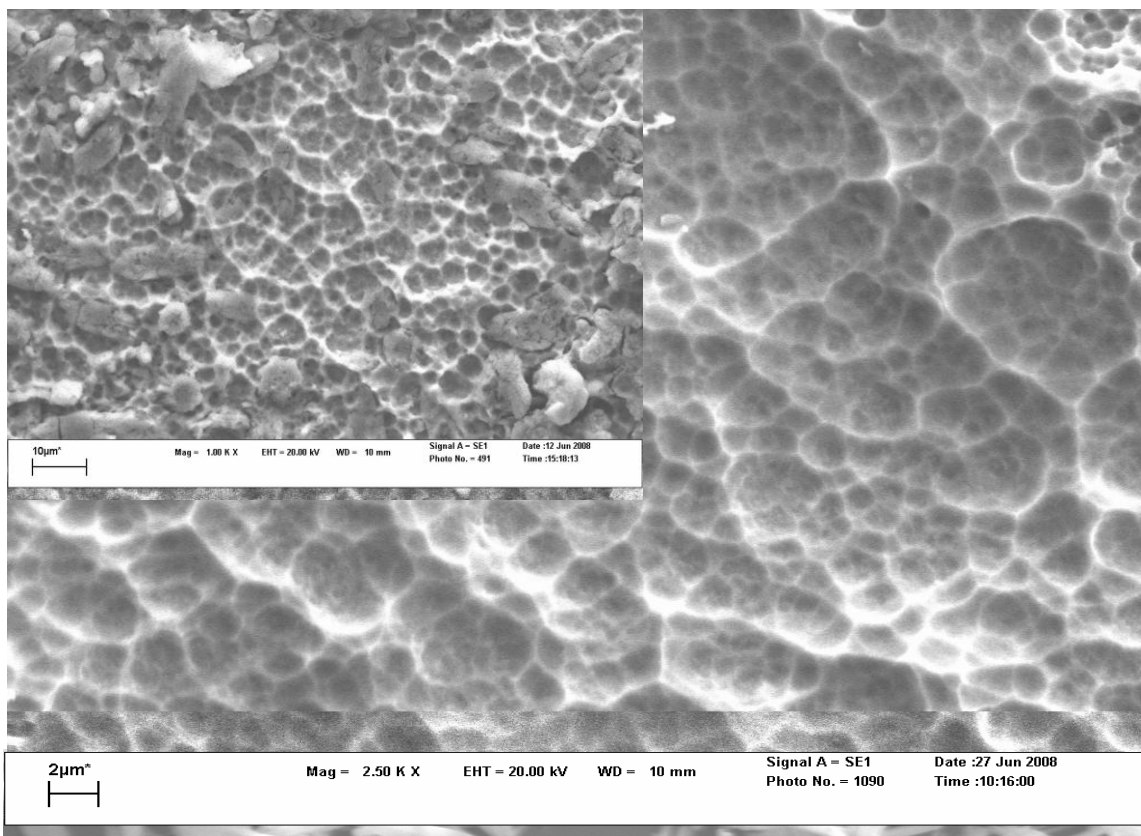


**Figure 1.** SEM image of oxidation in a strong acid on a Ti substrate [Route (i)].

In Figure 2, when zinc oxide was chemically grown on a titanium substrate [Route (ii)] various smooth rod shape architectures including star-shape and flower-like structures in the nanometer diameter scale were seen. The diameter of the rods ranges from 50 -150 nanometers and the lengths in excess from $1 - 2$ μm (figure 1 insert). Vayssieres et al [11-13] showed similar structures for zinc oxide growth on various substrates together with transparent conductive oxide, Si wafers, sapphire, polypropylene and glass. The authors controlled the shape and orientation of crystallites which consists of growing thin film materials directly onto substrates, from the molecular scale to the nano-/mesoscale, from aqueous precursors in solution by monitoring the thermodynamics and kinetics of nucleation and growth of the materials by controlling experimentally its interfacial tension. Figure 3 shows SEM micrograph using Route (iii) when sol-gel synthesis of $IrO_2$-$Ta_2O_5$ was carried out, followed by adsorption on the Ti substrate, after which oxidation of the Ti/$IrO_2$-$Ta_2O_5$ took place (insert figure 3). The micrograph showed heterogeneous cracked morphology consisting of flat, smooth areas and aggregated particles formed on smooth areas. These aggregated particles were attributed to $IrO_2$ and the flat area to the combination of both tantalum and iridium oxides. The SEM

results are also consistent with the view point of Roginskaya et al [21], who showed that the boundaries of $IrO_2$ crystallites were modified by $Ta_2O_5$ in mixed oxides. The finer the crystallites of $IrO_2$, the more pronounced the contributions of $Ta_2O_5$ modification to the mixed modified phase. There is a remarkable effect of Ta component on the crystallization dynamics of $IrO_2$ crystallite phase indicated by SEM results. Previous work [22 - 24] indicated that the crystallite size of the pure $IrO_2$ increased with annealing temperature. This indicates the possibilities of metal oxides rearrangement at higher temperatures, which includes metal oxide separations into separate crystalline domains.
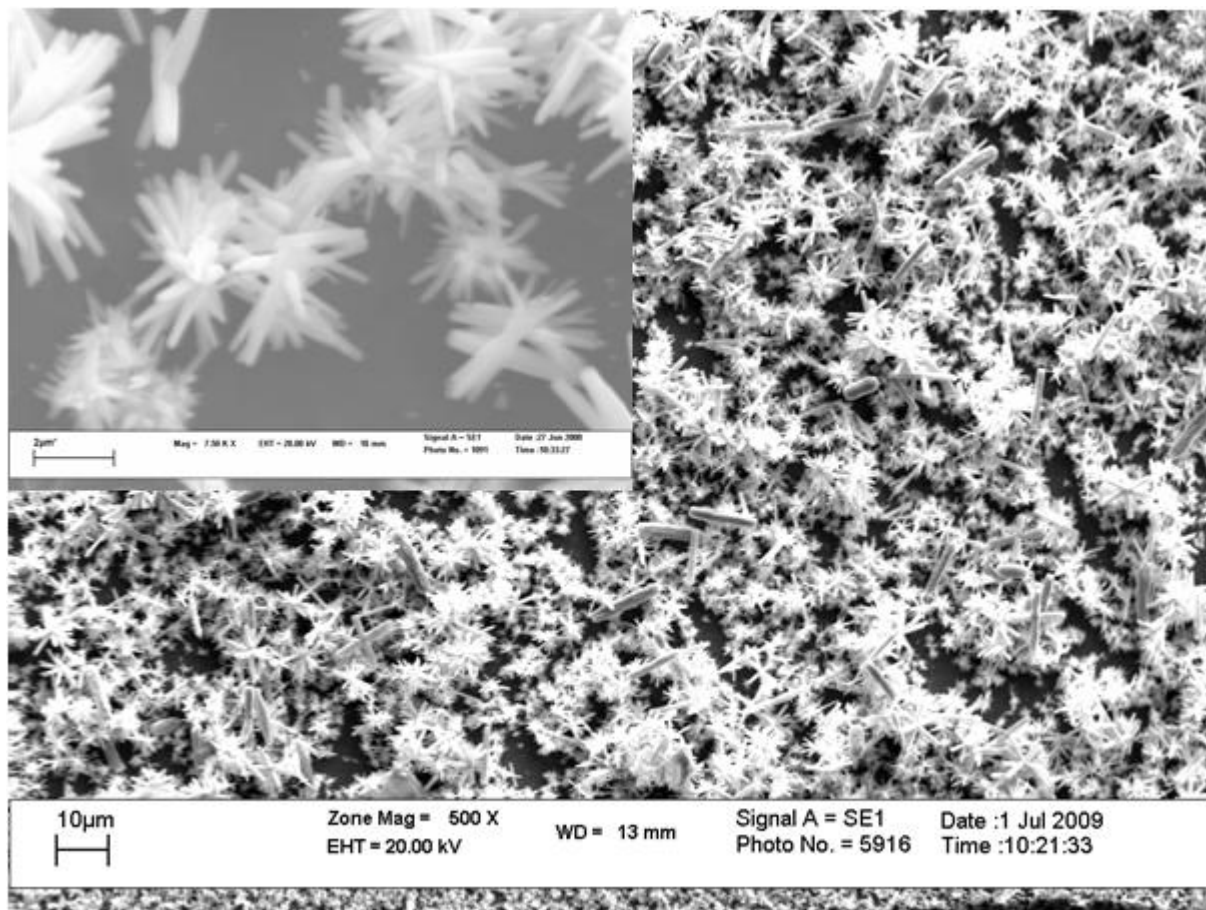


**Figure 2.** SEM image of ZnO on a titanium substrate [Route (ii)]

Figure 4 shows the structure of the $SnO_2$ -$RhO_2$ –$IrO_2$ on the surface of titanium substrates prepared as described in route (iv). The morphology of the surface layer of the modified Ti/$SnO_2$-$RhO_2$-$IrO_2$ electrode showed that oxide coating were heterogeneous presenting cracked-mud rough morphology which is flat and porous surface. The surface morphology of the thin film appeared to have cracked and porous regions. The pores are attributed to Rh, as Rh contents were increased, more pores were observed which exposed the Ti substrates, hence the formation of $TiO_2$ was observed. These results agree with those obtained by Crouch et al. [14, 15]. In this study ,the SEM cross sectional surface of Ti/$SnO_2$-$RuO_2$-$IrO_2$ thin film showed rough morphology with a network structure and porous surface with dimension range between 1.5 and 2μm in diameter. The film thickness was

also estimated to be ~1.6 μm which depended on the rate of dip coating and the side view indicated the formation of a homogeneous film [25].
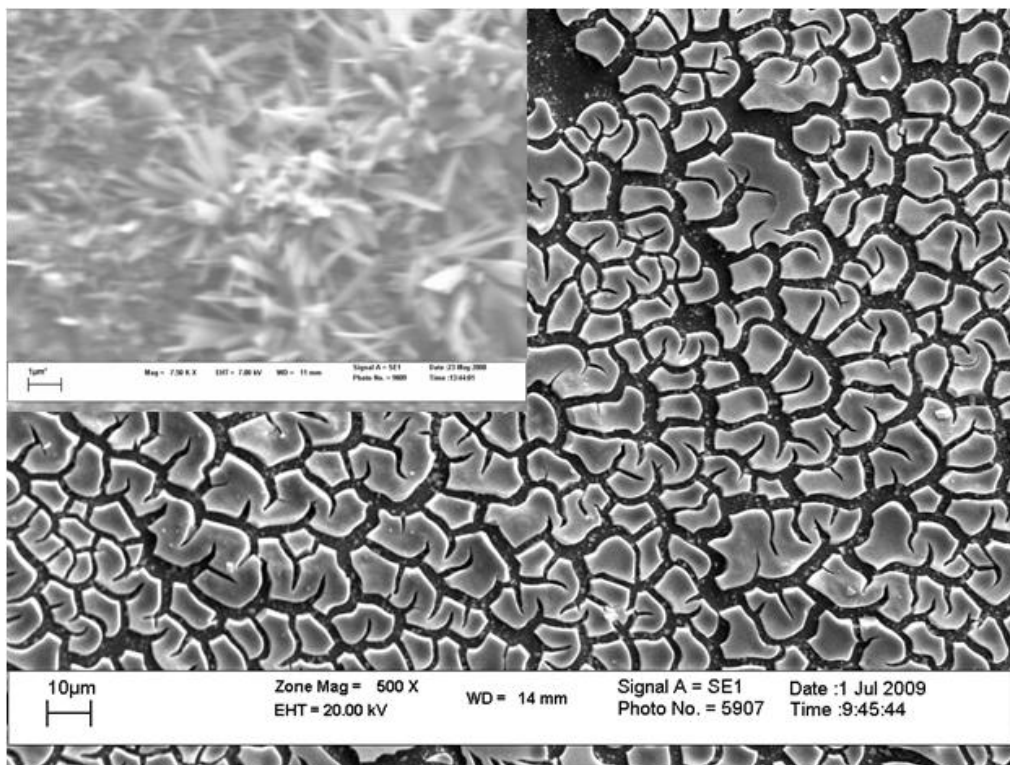


**Figure 3.** SEM image of $IrO_2$-$Ta_2O_5$ on a titanium substrate [Route (iii)].



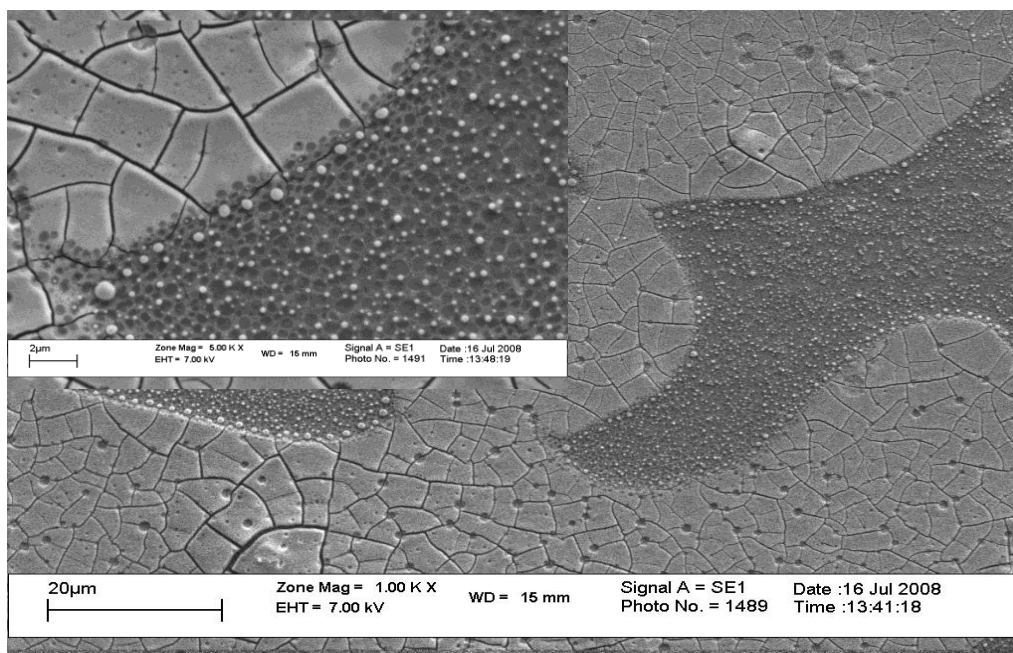**Figure 4.** SEM image of a $SnO_2$-$RhO_2$-$IrO_2$ sol-gel oxidation on a titanium substrate [Route (iv)]

Similar study was also carried by Talba et al. the authors also found that the SEM micrograph of the $SnO_2$-$IrO_2$ and $RuO_2$-$IrO_2$ on Titanium substrates with coating prepared by thermal decomposition on titanium support. These oxide coatings of Ti/$SnO_2$-$IrO_2$ and Ti/$RuO_2$-$IrO_2$ presented a similar cracked-mud structure. These were relatively flat, small and deep cracks with an average width of 2μm which surround the small 'islands'. The cracks were produced on the surface during the cooling of the electrode to room temperature [26 -27]. Table 1 below shows the elemental weight % of the different preparation routes.

**Table 1.** EDX Weight % of the different preparation routes

| Analysis | Weight% Si | Weight% P | Weight% Ti | Weight% Rh | Weight% Sn | Weight% Ta | Weight% Total |
|---|---|---|---|---|---|---|---|
| Sample Route iii | | | 99.75 | | | 0.25 | 100.00 |
| Sample Route iv | | 6.04 | 88.65 | | 4.51 | 0.79 | 100.00 |
| Sample Route iii | 0.29 | 0.83 | 64.14 | 34.74 | | | 100.00 |
| Sample Route i | 1.60 | 0.50 | 97.83 | 0.07 | | | 100.00 |
| Sample Route iv | 0.25 | 1.41 | 85.21 | 13.12 | | | 100.00 |
| | | | | | | | |
| Analysis | Weight% Ti | Weight% Zn | Weight% Ru | Weight% Sn | Weight% Ta | Weight% Ir | Weight% Total |
| Sample Route iii | 75.85 | | | | 0.73 | 23.43 | 100.00 |
| Sample Route iv | 60.15 | | 12.91 | 26.75 | | 0.19 | 100.00 |
| Sample Route i | 100.00 | | | | | | 100.00 |
| Sample Route iii | 99.41 | | 0.49 | 0.10 | | | 100.00 |
| Sample Route ii | 39.32 | 60.69 | | | | | 100.00 |

*3.2 Atomic Force Microscopy (AFM)*

Atomic Force Microscopy (AFM) was employed for the characterization of the different mixed metal oxides on titanium substrates synthesized by routes (iii) and (iv). Atomic force micrographs of the different mixed metal titanium metal oxide synthesized routes showed different surface roughness. Samples prepared as described in route (iv) were observed to have greater surface roughness as compared to those prepared by route (iii). The Atomic Force Microscopy (AFM) was employed to detect structures, chemical interactions and forces in the nanoscale range. Figure 5 shows the atomic

force micrograph of the Ti/IrO$_2$ –Ta$_2$O$_5$ (route iii) electrode measured from the dark spot to the light spot on the film. The film displayed rough and micro porous surface whose lateral diameter varies typically between 50 - 200 nm and is in 120-250 nm range.
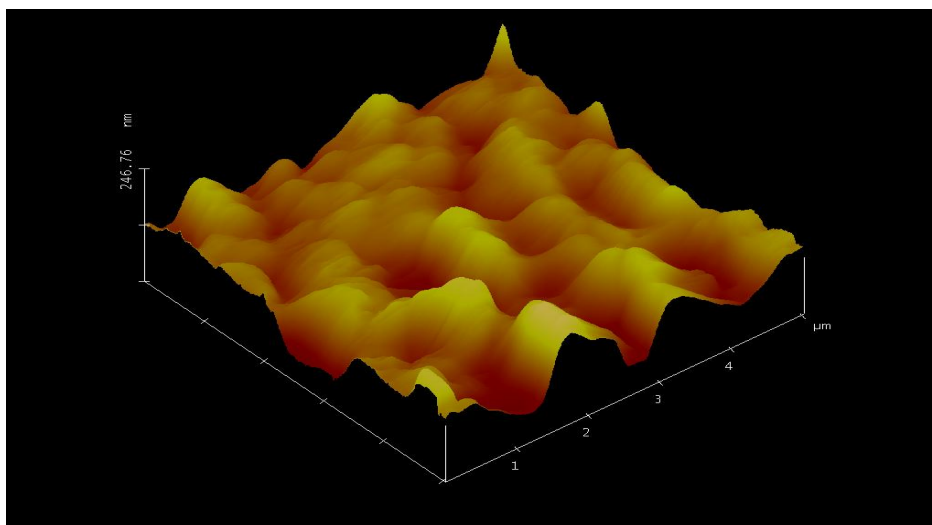


**Figure 5.** AFM of IrO$_2$-Ta$_2$O$_5$ on a titanium substrate prepared using Route (iii)

The AFM of SnO$_2$-RhO$_2$-IO$_2$ (route iv), (Fig. 6) show a good definition of the surface area roughness and average depth profile of the pores with nanosizes peaks and pits. The nanosized peaks estimated between 100 and 400 nm and the depth of nanopits were 500 nm in height. Measurements were also made from the low point (dark spot) to the (light spot) on the film. Baker et al. in their study concluded that dip coated samples were observed to have greater surface as compared to the sample prepared by spin coating [14, 28].
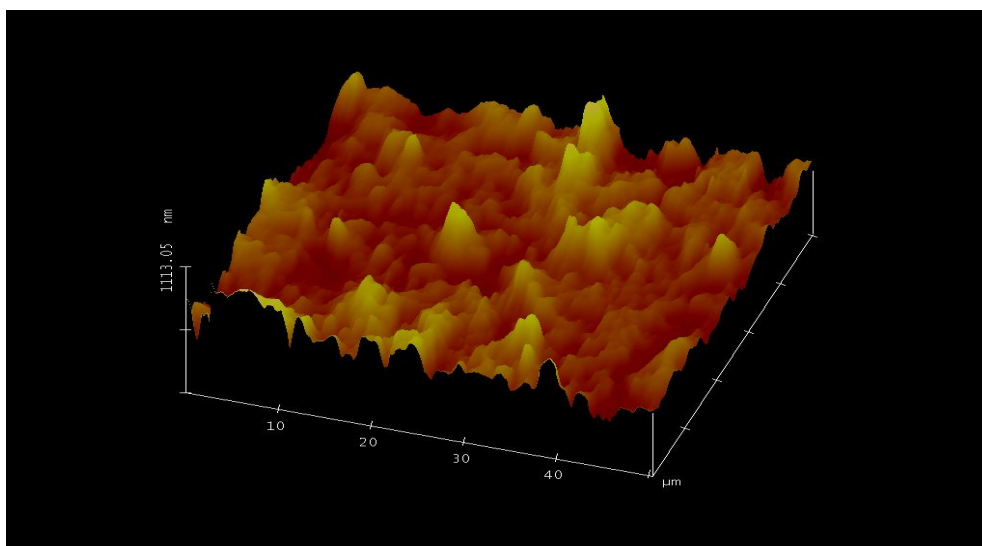


**Figure 6.** AFM of SnO$_2$-RhO$_2$-IO$_2$ sol-gel oxidation on a titanium substrate prepared using Route (iv)

*3.3 X-ray Diffraction Microscopy (XRD)*

X- Ray Diffractometry (XRD) was employed to confirm the crystalline nature of the structure of the oxide films coated on the titanium substrates. The XRD patterns of the ZnO nanostructures showed the diffraction peaks which can be indexed as the hexagonal wurtzite structure. No characteristic peaks of other peaks such as Zn were observed.
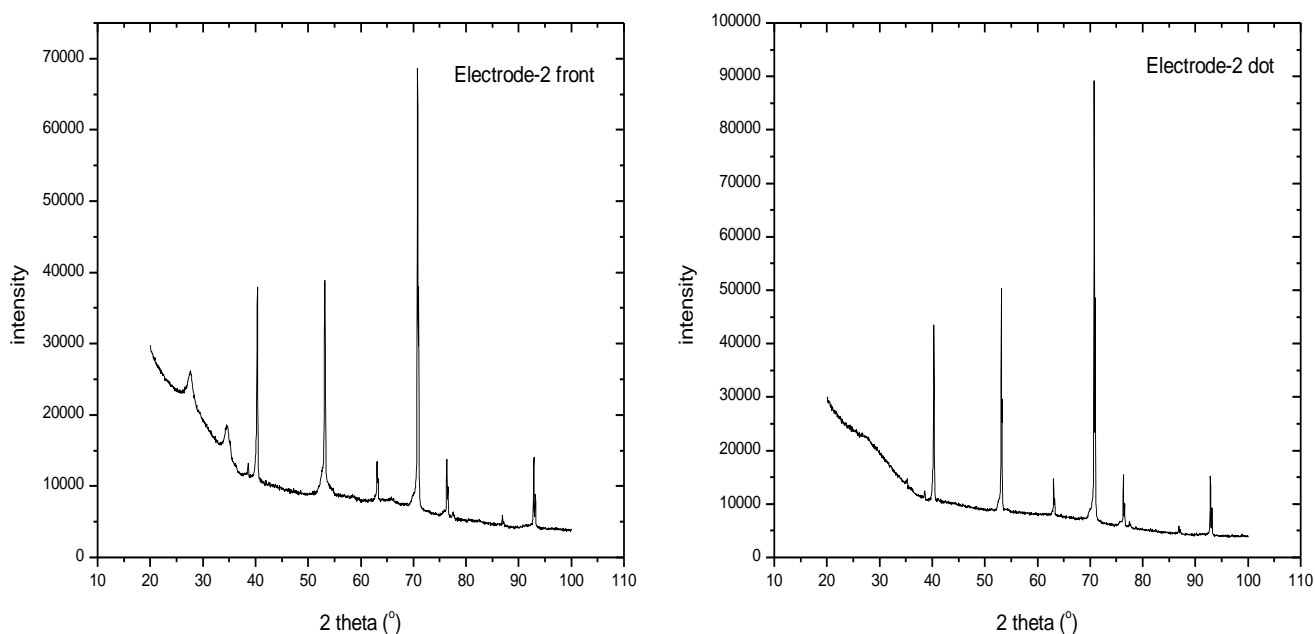


**Figure 7.** XRD pattern of $Zn(NO_3)_6.6\ H_2O$ at low temperatures on Titanium substrates (route ii)
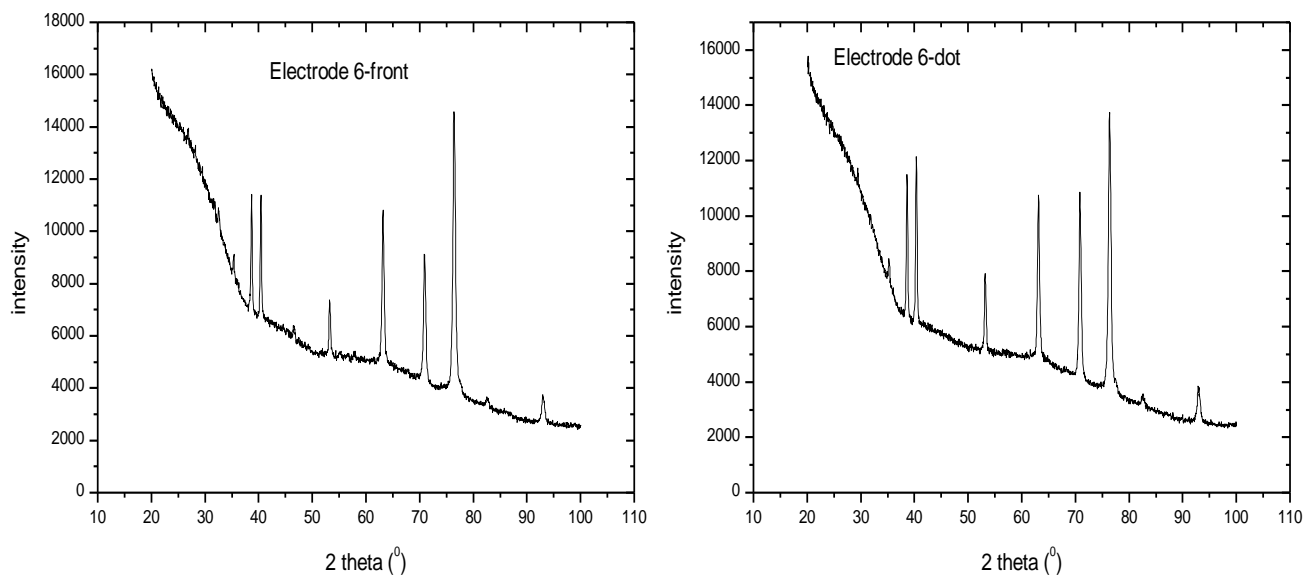


**Figure 8.** XRD pattern of $IrO_2$- $Ta_2O_5$ oxidation on Titanium substrates (route iii)

According to the intensity and width of the XRD pattern, this reveals that even if the electrode was synthesized at low temperature the sample still have a well-defined crystalline structure and morphology in the presence of surfactant which is capable of increasing the response of the sensing material (Figure 7) [29-30]. Note that electrode front is the front part of the electrode and electrode dot is the back part of the electrode

Figures 8 and 9 shows the X-ray diffractograms of the surface composition of the Ti/ $Ta_2O_5$–$IrO_2$ electrodes synthesized by using routes (iii) and (iv). As can be seen from the figures the surface composition are different with the difference in the preparation routes of the electrodes though they all show the $IrO_2$ peaks being fairly narrow and strong. This suggested good crystallinity of $IrO_2$. The segregated crystallites on the coating surface were considered to enrich $IrO_2$ rutile. Diffraction peaks corresponding to the Ti support were also observed which came from the penetration of the X-ray to reach the substrates in some thin areas. The $Ta_2O_5$ peaks were not that obvious because the coating and the intensity were not strong.

Similar study was also carried out by Bao-song et al[26]. They investigated the $IrO_2 - Ta_2O_5$ on titanium substrates with the variation of $IrO_2$ and observed that the number of crystallite phase vary with the content ratio of Ir to Ta. $IrO_2$ contents are up to 55%, the crystallite phase in the mixture existed entirely as rutile phase and none of the amorphous $Ta_2O_5$ peaks were detected. They concluded that the crystallization of $Ta_2O_2$ is affected by the $IrO_2$ components [28].
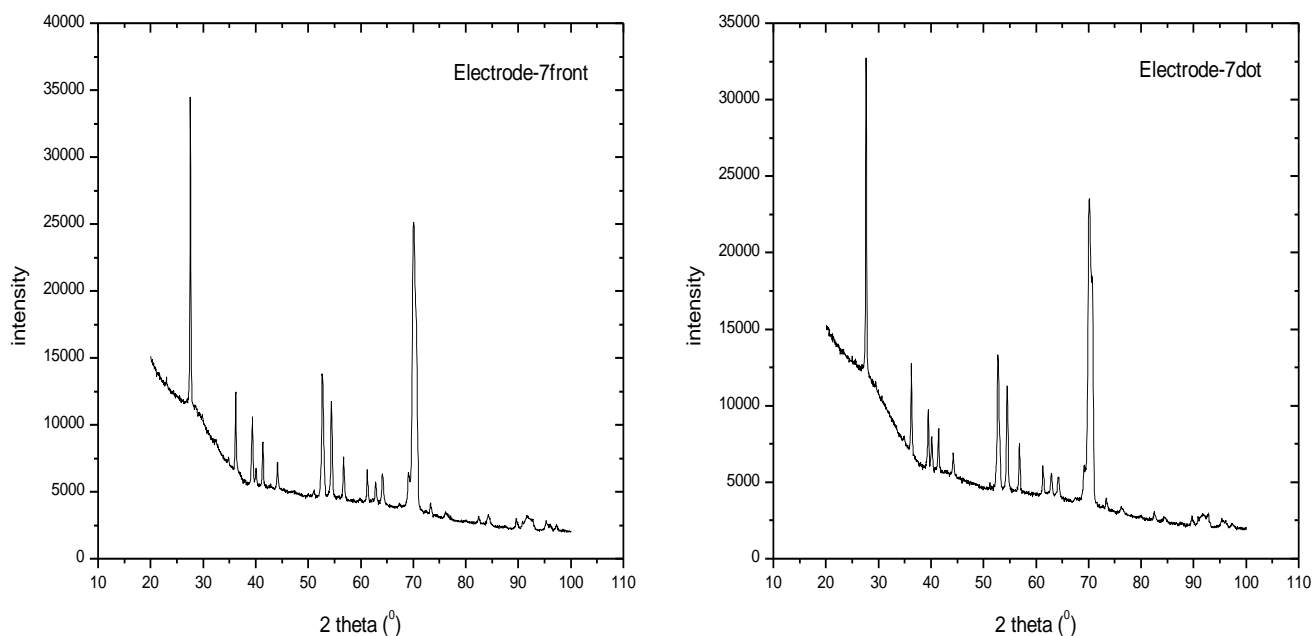


**Figure 9.** XRD pattern of $IrO_2$- $Ta_2O_5$ sol-gel on titanium substrate (route iv)

The XRD pattern of the Ti/ $SnO_2$- $RhO_2$- $IrO_2$ electrode were also recorded (not shown here). The matching of the observed values confirmed that the deposited film consist of cassiterite $SnO_2$ and

rutile IrO$_2$ tetragonal structures. The metallic titanium (Ti) crystalline peaks observed in pattern were due to the titanium substrates, the X-ray penetration through to the substrates [31-32].

## 5. CONCLUSIONS

This investigation shows that binary and ternary metal oxide nanostructures can be synthesized on a titanium substrate using different preparation routes. SEM micrographs showed different morphologies for the binary and ternary metal oxide structures for the different preparation routes: TiO$_2$ nano-pores with a broad range of scales between 20 – 120 nm and an inner diameter wall of 5 – 15 nm inner circle thickness were observed (route i); the diameter of the ZnO rods ranged from 50 - 150 nm and the lengths in excess from 1 – 2 μm (route ii); a heterogeneous cracked morphology consisting of flat, smooth areas and aggregated particles formed on smooth areas (route iii) and heterogeneous cracked-mud rough morphology which is flat and porous surface (route iv) . AFM displayed rough and micro porous surface with lateral diameter varying typically between 50 - 200 nm and is in 120-250 nm for Ti/IrO$_2$ –Ta$_2$O$_5$ and the peaks ranged range between 100 and 400 nm and the depth of nanopits were 500 nm in height for Ti/SnO$_2$ - RhO$_2$- IrO$_2$. XRD distinctively identified the presence of crystalline structures of IrO$_2$, SnO$_2$ and ZnO modified electrodes.

## References

1.  R. Berenguere, C. Quijada, E. Morallon, *Electrochimica Acta* 54 (2009) 5230.
2.  W.S. Oh, C. Xu, D.Y. Kim, D.W. Goodman , *Journal of Vacuum Science and Technology A* 15 ( 3) (1997) 1710.
3.  H. Kim, W. Son, T. Kim, K. Kang, T. Osaka, S. Park, *Jour. of European Ceramic Society.* 27 (2007) 3749.
4.  L. Lipp, D. Plecher, *Electrochimica Acta* 42 (7) (1997). 1091
5.  M. Aronniemi, J. Saino, J. Lautinen, *Thin Solid Films* 516 (2008) 6110.
6.  P.A. Cox, *Transition metal oxides*, Clarendon Press, Oxford, 1995.
7.  J.B. Goodenough, *Prog. Solid State Chemistry*, 5 (1971) 145.
8.  N.N. Greenwood, A. Earushaw, *Chemistry of Elements,* Pergamon Press, Oxford, 1984.
9.  S. Trasatti, *Electrodes of Conductive Metallic Oxides*: Part B, Elsevier Scientific Publishing, New York, 1981.
10. Q. Cai, M. Paulose, O.K. Varghese, C.A. Grimes, *J. Mater. Res.* 20 (2005) 230.
11. L. Vayssieres, K. Keis, S. –E. Lindquist, A. Hagfield, *J. Phys. Chem. B* 105(2001) 3350
12. L. Vayssieres, L. Rabenberg, A. Manthiram, *Nano Lett.* 2 (2002) 1393
13. L. Vayssieres *Adv. Mater.* 15(2003) 464
14. P.G.L. Baker, R.D. Sanderson, A.M. Crouch, *Thin solid films* 515 (2007) 6691.

15. M.E. Makgae, C.C. Theron, W.J. Prybylowicz, A.M. Crouch, *Mater. Chem. Phys.* 92 (2005) 559.
16. G.K. Mor, O.K. Varghese, M. Paulose, N. Mukherjee,C.A. Grimes, *J. Mater. Res.* 18 (2003) 2588.
17. K.S. Raja, M. Misra, K. Paramguru, *Electrochim. Acta* 51 (2005) 154.
18. K. Yasuda, J.M. Macak, S. Berger, A. Ghicov, P.Schmuki, *J. Electrochem. Soc.* 154 (2007) C472.
19. S. Joo, I. Muto, N. Hara, *J. Electrochem. Soc.* 155 (2008) C154.
20. G.A. Crawford, N. Chawla, *Scripta Materialia* 60 (2009) 874.
21. Y.E. Roginskaya, O.V. Morozova, *Electrochimica Acta.* 40(7) (1995) 817.
22. Y. Murakami, S. Tsuchiya, K. Yahikozawa, Y. Takasu, *Electrochimica Acta.* 39 (5) (1994) 651.
23. T.Y. Wang, L.K. Xu, G.Z. Chen, *Acta Metallurgica Sinica.* 14 (6) (2001) 457.
24. Y. Fiamegos, C. Stalikas, G. Pilidis, *Analytica Chimica Acta.*467 (1-2) (2002) 105.
25. K.N. Kuromoto, R.A. Simao, G.A. Soares, *Material Characterization* 58 (2007) 114.
26. L. Bao-song, L. An, G. Fu-xing, *Trans.Nonferrous Met.Soc.China.*16 (2006) 1193.
27. R. Talba, M. Tian, J. Wen, Z. Jaing, A. Chen, *Journal of Electroanalytical Chemistry* 649 (1-2) (2010) 9.
28. T. Bezrodna, G. Puchkovska, V. Shymanovsvska, A. Hanser, A. *Jour. of Physics and Chemistry of Solids* 66 (2005) 1057.
29. S.K. Panda, C. Jacob, *Physica E* (2009) 792 - 796
30. P. Sangpour, M. Roozbehi, O. Akhavan, A. Z. Moshfegh, *Current Nanoscience* 5 (2009) 479.
31. M. Batzill, U. Diebold, *Progress in Surface Science* 79 (2005) 47.
32. L. C. Nehru, V. Swaminathan, M. Jayachandron and C. Sanjeeviraja, *Materials Science Forum* 671 (2011) 69.